Applied Thermal Engineering 159 (2019) 113878

Contents lists available at ScienceDirect

Applied Thermal Engineering

journal homepage: www.elsevier.com/locate/apthermeng

Numerical and experimental investigation on the condensing heat transfer of R134a outside plain and integral-fin tubes

Wen-Tao Ji[a,*], Shuai-Feng Mao[a], Guo-Hun Chong[a], Chuang-Yao Zhao[a], Hu Zhang[b], Wen-Quan Tao[a]

[a]Key Laboratory of Thermo-Fluid Science and Engineering of MOE, Xi'an Jiaotong University, Xi'an 710049, China
[b]State Key Laboratory of Strength and Vibration of Mechanical Structures, School of Aerospace, Xi'an Jiaotong University, Xi'an, 710049, China

HIGHLIGHTS

- Numerical results of plain and 32-fpi tube agree well with experimental data.
- An increase in film thickness at root fin was observed with increasing fin density.
- Condensing HTCs of lateral and root fin decrease as temperature difference reduces.

ARTICLE INFO

Keywords:
Condensation
Tube
Heat transfer enhancement
VOF
CFD

ABSTRACT

Condensing heat transfer of R134a on horizontal single plain and integral-fin tubes was investigated by both computational and experimental methods. The VOF model and Lee condensation model were utilized in the simulation. Validation of the model was performed with two different refrigerants. Condensing heat transfer coefficient for plain and integral-fin tubes were calculated in comparison with the experimental data and Nusselt analytical solution. Instantaneous film flow characteristics of condensation on horizontal single plain and integral-fin tubes were discussed respectively. Contours of liquid volume fraction for the plain tube and condensing heat transfer coefficient for the plain tube at different time with T_w = 303 K are presented. For integral-fin tubes, contours show that the thickness of liquid film at lateral fin surface is much smaller than that at root fin surface. Comparison between R134a and R11 were made and it was found that different surface tension could lead to different liquid film distribution which could result in different heat transfer performance. Experiments involving the same fin structure were also conducted to verify the theoretical model and a satisfactory agreement between simulation and experimental results was found.

1. Introduction

Film-wise condensation outside horizontal tubes occurs frequently in power, chemical process and air-conditioning systems. Plain tubes were firstly used in the shell and tube condensers. Nusselt analytical solution can be used to predict the condensing heat transfer coefficient of vapor outside the single horizontal plain tube [1]. It has been proved to be accurate for different types of refrigerants. Integral-fin tube was used in condensing applications since 1940s and founded to be effective in the shell and tube condensers. Many experiments have been conducted to test the condensing heat transfer outside the integral-fin tubes. Cheng and Wang [2] measured the condensing heat transfer coefficient of R134a outside three integral-fin tubes. They found that the Beatty and Katz model under-predicts the condensing heat transfer coefficient for integral-fin tubes by as much as 54% and pointed out that this model can't be applied to integral-fin tubes with high fin density.

In order to obtain optimum fin density for the condensation of R134a on low-finned tubes, Zhang et al. [3] conducted the experiment of film condensation of R134a on single horizontal plain tube and five low-finned tubes. They found that the optimum fin density for R134a is 55 FPI (fins per inch) outside low-finned tubes. Ji et al. [4] tested the enhanced tubes including integral-fin, pyramid and re-entrant cavity surface with the heat flux ranging from 8 to 86 kW/m^2. The condensing heat transfer coefficients can be 14.8–19.3 times those of plain tube. They also experimentally investigated the condensation of R134a on a single, high-density, low-fin tube and full-sized shell and tube condensers [5].

* Corresponding author.
E-mail address: wentaoji@xjtu.edu.cn (W.-T. Ji).

https://doi.org/10.1016/j.applthermaleng.2019.113878
Received 6 November 2018; Received in revised form 19 May 2019; Accepted 27 May 2019
Available online 28 May 2019
1359-4311/

Nomenclature

List of symbols

T_w	tube wall temperature, K
T_s	saturation temperature, K
h	condensing heat transfer coefficients, $W{\cdot}m^{-2}{\cdot}K^{-1}$
C_n	enhanced ratio
q	heat flux, $W{\cdot}m^{-2}$
T	time, s
D	diameter, mm
H	fin height, mm
P_f	fin pitch, mm
g	gravitational acceleration, $m{\cdot}s^{-2}$
t	positive numerical coefficient, s^{-1}
S_l	mass source due to phase change, $kg{\cdot}m^{-3}{\cdot}s^{-1}$
h_{latent}	latent heat, $J{\cdot}kg^{-1}$
r	latent heat in Eqs. (18), (19), $J{\cdot}kg^{-1}$
d	diameter in Eqs. (18), (19), mm
F_σ	surface tension in Eqs. (7) and (8)

Greek alphabet

α_l	volume fraction of liquid
α_v	volume fraction of vapor
ρ	density, $kg{\cdot}m^{-3}$
κ	interface curvature, m^{-1}
λ	thermal conductivity, $W{\cdot}m^{-1}{\cdot}K^{-1}$
μ	dynamic viscosity, Pa·s
σ	surface tension, $N{\cdot}m^{-1}$

The effect of condensate inundation on film condensation of R134a for tube bundles was studied by Gstoehl et al. [6]. They found that the increasing inundation rate will deteriorate the condensing heat transfer of 3D enhanced tubes while it has little effect on the heat transfer coefficient of the low fin tube.

The influence of fin structure and density on the condensation heat transfer of R134a was experimentally investigated by Al-Badri et al. [7]. Condensing heat transfer coefficient of enhanced finned tubes with 39, 48, and 56 FPI and different fin heights was tested in comparison with the standard one. The result shows that the tube with 48 FPI and larger fin height has the highest condensing heat transfer coefficient compared with other standard finned tubes. Recently, the heat transfer performance of some new refrigerants was also tested. External condensing heat transfer coefficients of R134a and R1234yf were measured on a plain, low fin, and Turbo-C tubes by Park et al. [8].

Gebauer et al. [9] tested the condensing heat transfer coefficient of R134a and R290 on coated and uncoated horizontal plain, standard finned and high performance tubes. Numerical simulation was used in Gebauer's work to predict the condensing heat transfer on single tubes for the first time to the author's knowledge. The volume of fluid (VOF) model was used in the numerical simulation to model the multiphase flow. The static condensation retention angle was investigated in their first adiabatic simulation and the average deviation compared with the analytical equation was less than 10% for integral-fin tubes. The condensing heat transfer coefficient of numerical simulation for the standard finned tube agreed very well with experimental results while for the high performance tube, the deviation was more than 21.5%. Zhao et al. [10] investigated the influence of surface structure and thermal conductivity on the condensation heat transfer of R134a and R404A outside single horizontal enhanced tubes. They found that the lower material thermal conductivity had a lower condensation heat transfer coefficient for the enhanced tubes, because of its smaller sub-cooling temperature distribution.

Many semi-empirical models were also proposed to predict the condensing heat transfer coefficients for the horizontal integral-fin tubes [11]. Beatty and Katz [12] also developed a theoretical model for a horizontal integral-fin tube. Based on the assumption that the force of gravity dominates condensate drainage, their model is suitable for tubes of low fin density and low-surface-tension fluids. Honda et al.'s [13] model can be used to predict the row-row heat transfer coefficient for downward flowing vapor on tube bundles. Webb et al. [14] took the surface tension into consideration and developed a theoretical model for both high and low surface tension fluids. The mean deviation between the values predicted by this model and the experimental data is within 20%. Murata and Hashizume [15] put forward a method predicting the condensing heat transfer coefficient outside the integral-fin tube bundles which also take the condensate inundation into account. Recently, Al-Badri et al. [16] calculated the condensing heat transfer coefficient for a finned tube by an analytical model. The model divided the tube into small annular elements, considering both the gravity and surface tension. The model agreed well with the experimental data with a mean deviation of 4.7%. These models should be helpful for the design.

Literature review shows that there are many experimental or theoretical investigations on the condensing heat transfer of refrigerant outside the enhanced tubes, while the studies with numerical simulations are quite few to the author's knowledge. Quantitative analysis on the condensate retained in the fin gaps plays an important role in identifying the heat transfer coefficient of enhanced tubes. But it is difficult to observe with the experimental method. In order to numerically investigate the refrigerant vapor condensing outside the enhanced tubes, VOF model were utilized in this paper to predict the condensing heat transfer outside the various finned tubes. Experiments involving the same fin structure were also conducted to verify the theoretical model.

The rest sections are arranged as follows: firstly, the mathematical formulation and numerical method are introduced; then the results and discussion are provided including comparison with the experiment, instantaneous film flow characteristics in condensing and condensing heat transfer coefficient in different locations of fins. Finally, some conclusions are summarized.

2. Mathematical formulation

2.1. Governing equations

Volume of fluid (VOF) model proposed by Nichols and Hirt [17,18] can generally be used to tracking the motion of the interface, e.g. the motion of a large bubble in liquid and the motion of liquid after dam break. Although there are some limitations, it is a simple and efficient means for numerically treating of free boundaries. The VOF model in Fluent 15.0 is used to simulate the condensation and flow outside the different types of tubes. For two-phase flow, α_l *and* α_v represent the volume fraction of liquid and vapor respectively in VOF model. Total volume fractions of liquid and gas should be constrained to 1:

$$\alpha_l + \alpha_v = 1 \tag{1}$$

The density ρ is calculated as follows:

$$\rho = \alpha_l \rho_l + \alpha_v \rho_v \tag{2}$$

Other thermal properties (e.g. viscosity and thermal conductivity) are also computed by means of arithmetic mean as shown in the above equations.

Energy and temperature are calculated as follows:

$$E = \frac{\alpha_l \rho_l E_l + \alpha_v \rho_v E_v}{\alpha_l \rho_l + \alpha_v \rho_v} \tag{3}$$

$$T = \frac{\alpha_l \rho_l T_l + \alpha_v \rho_v T_v}{\alpha_l \rho_l + \alpha_v \rho_v} \tag{4}$$

The governing equations including continuity, momentum, energy conservations are as follows:

Continuity equation:

$$\frac{\partial(\alpha_l \rho_l)}{\partial t} + \nabla\cdot(\alpha_l \rho_l u) = S_l \tag{5}$$

$$\frac{\partial(\alpha_v \rho_v)}{\partial t} + \nabla\cdot(\alpha_v \rho_v u) = -S_l \tag{6}$$

where S_l is the mass source term (kg/m^{3}s) that is obtained from the condensation model.

Momentum equation:

$$\frac{\partial(\rho u)}{\partial t} + \nabla\cdot(\rho u u) = -\nabla p + [\mu(\nabla u + \nabla u^T)] + \rho g + F_\sigma \tag{7}$$

where p is the pressure. The continuum surface force (CSF) model proposed by Brackbill et al. [19] is used to calculate the surface tension.

$$F_\sigma = \sigma \kappa \nabla \alpha_l \frac{\rho}{1/2(\rho_l + \rho_v)} \tag{8}$$

$$\kappa = \nabla\cdot\left(\frac{\nabla \alpha_l}{|\nabla \alpha_l|}\right) \tag{9}$$

where κ is the curvature and σ represents the surface tension coefficient.

Energy equation:

$$\frac{\partial(\rho E)}{\partial t} + \nabla\cdot[u(\rho E + p)] = \nabla\cdot(\lambda \nabla T) + S_l h_{latent} \tag{10}$$

where h_{latent} is the latent heat.

2.2. Condensation model

In the numerical investigation, it takes both the heat and mass transfer into account. The mass source term was calculated by a phase-change model proposed by Lee [20]. The Lee condensation model coupled with VOF model has been widely used in modeling flow condensation in tubes. Qiu et al. [21] performed a numerical study on the condensation flow of hydrocarbon mixtures inside the tubes of liquefied natural gas coil-wound heat exchangers. Their numerical results using VOF model coupled with Lee model showed a good agreement with experimental results. The relative errors of void fraction, heat transfer coefficient and frictional pressure drop were within 5%, 15% and 15%. Another numerical investigation on flow condensation of zeotropic hydrocarbon mixtures in a helically coiled tube was performed by Yu et al. [22]. VOF model coupled with Lee model were used in their simulation to obtain the flow pattern and heat transfer coefficient. Based on the numerical results, a new correlation for heat transfer coefficient were proposed with a mean absolute relative deviation of 9.2%.

The mass transfer in Lee model can be described as:

$$\begin{cases} S_v = t\cdot\alpha_l \rho_l \frac{T_l - T_{sat}}{T_{sat}} & T_l > T_{sat} \text{(evaporation)} \\ S_l = t\cdot\alpha_v \rho_v \frac{T_{sat} - T_v}{T_{sat}} & T_v < T_{sat} \text{(condensation)} \end{cases} \tag{11}$$

where T_{sat} is the saturation temperature, T_l is liquid temperature, T_v is vapor temperature, S_v is the mass transfer in evaporation and S_l is the mass transfer in condensation. At a certain computational step, if the temperature of liquid cell is higher than the saturation temperature, Eq. (11) is used. It should be noted that no mass transfer will be computed if the cell belongs to vapor. Additionally, if the temperature of the cell decreases, it is because of the energy source term $S_l h_{latent}$ existed in the energy equation which denotes the heat transfer. For the vapor cell, when its temperature is lower than the saturation temperature, Eq. (11) is used.

The t is a coefficient which can be interpreted as relaxation time (1/s). Based on the kinetic theory of evaporation-condensation and Hertz Knudsen equation [23], it is defined as:

$$t = \frac{6}{d_b}\beta\sqrt{\frac{M}{2\pi R T_{sat}}}L\left(\frac{\alpha_v \rho_v}{\rho_l - \rho_v}\right) \tag{12}$$

However, it is hard to calculate t by the expression because β is usually unknown. It is important to tune the value of t. It has been proved that too large value of t could result in convergence problem and too small value may result in large deviation between interfacial temperature and saturate temperature. Da and Del [24] performed the condensation simulation for simple cases with different values of coefficient t. Their results show that by increasing the value of coefficient t, the interfacial temperature gets closer to the saturation temperature. Besides, they point out that too large value of t results in convergence problems. The value of t depends on particular cases and should be finely tuned. They finally used the coefficient $t = 750000\,s^{-1}$. In the present numerical study, the coefficient $t = 50000\,s^{-1}$ was adopted and the interfacial temperature was equal to saturation temperature.

3. Numerical method

3.1. Physical model

This numerical study focuses on a single horizontal plain and a single horizontal integral-fin tube in the condenser full of refrigerant vapor. Fig. 1(a) illustrates the geometry of the integral-fin tube, the domain (Fig. 1(b)) between the fins is selected as calculation domain. As shown in Fig. 1(c), the surface outside integral-fin tubes can be divided into three parts: lateral fin, root fin and fin tip. In seek of an accurate calculation, structured grid shown in Fig. 1(d) was used in numerical simulation for plain and integral-fin tubes. The specifications of tubes in numerical simulation are given in Table 1.

3.2. Assumptions and solution method

The following assumptions were made for the present numerical simulation:

(1) The thermo-physical properties are constant.
(2) The temperature on the vapor-liquid interface is nearly saturated.
(3) The thicknesses of tube and condensate inundation are ignored.
(4) The flow of liquid condensed outside the tube is laminar.

The boundary condition along the tube is uniform temperature. Pressure outlet boundary condition was applied for the bottom of condenser. The velocity inlet was applied for the upper of the condenser, and the inlet of liquid was set to zero. Two symmetry surfaces were used to reduce calculation time. No-slip condition was applied at the wall.

The simulation of condensation was performed on ANSYS Fluent 15.0 CFD commercial package. Pressure-based solver was used for the flow. The SIMPLE (Semi-Implicit Method for Pressure Linked Equation) scheme was used for pressure-velocity coupling while pressure discretization was handled by the PRESTO! (Pressure Staggering Option) scheme. The third order MUSCL scheme [25] was used to discretize momentum and energy equations. Least Squares Cell based and Quick (quadratic upwind interpolation of convective kinematics) algorithm were implemented for gradient and volume fraction discretization respectively. Transient formulation is discretized using second order implicit scheme. The convergence criterion was set at 10^{-5} for energy equation and 10^{-3} for all the other equations.

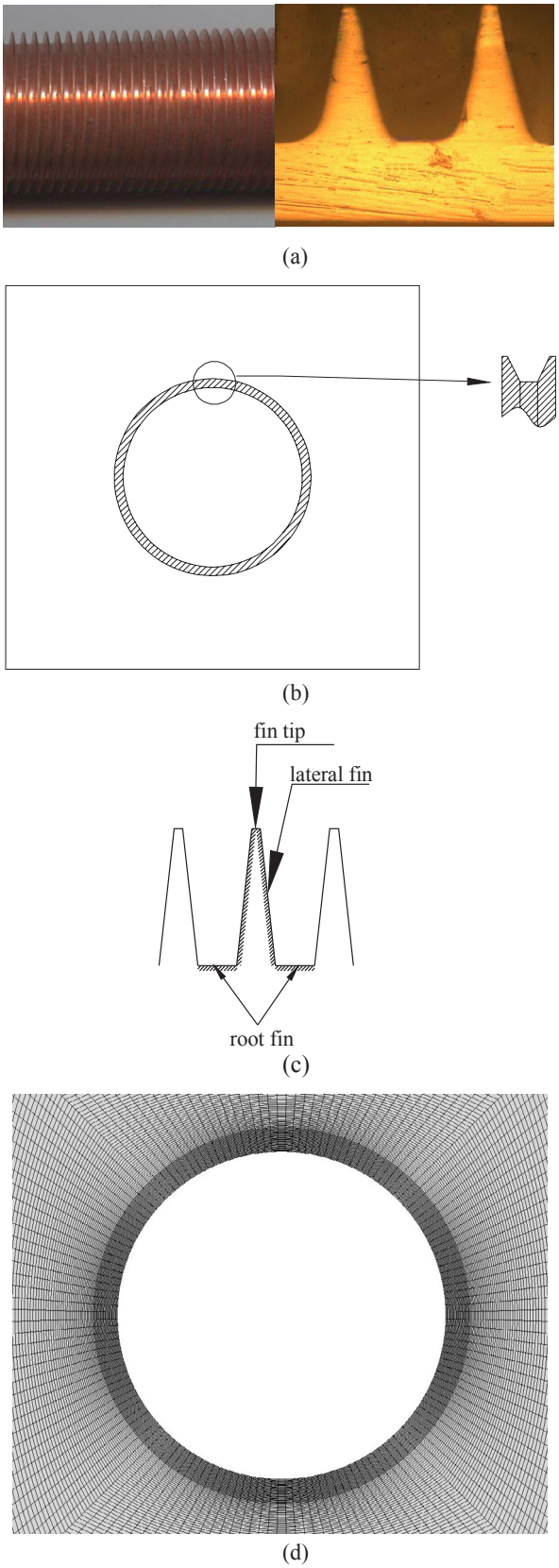

Fig. 1. Schematic of fins and grid system. (a) Geometrics of integral-fin tube, (b) schematics of the calculation domain fin tip, (c) schematics of the fins, and (d) schematics of grid system.

Table 1
Specifications of the tubes in numerical simulation.

Tube designation		Plain tube	26 fpi	32 fpi	41 fpi
Fin pitch (P_f)	mm	–	0.97	0.79	0.61
Fin height (H)	mm	–	1.4	1.4	1.4
Tube outside diameter (D)	mm	19	19	19	19

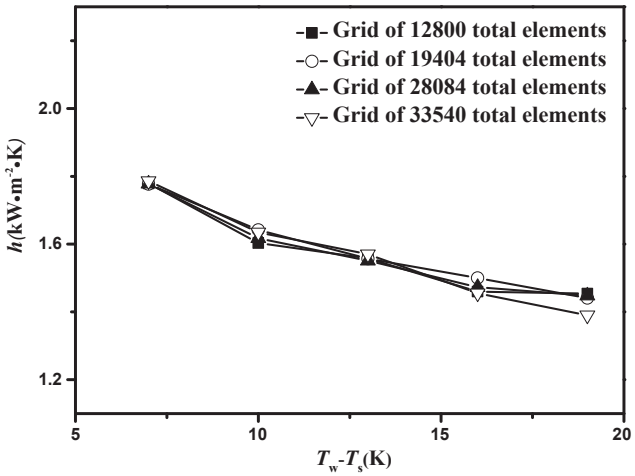

Fig. 2. Variation of the condensing heat transfer coefficient with grid number.

4. Results and discussion

4.1. Grid independence

The grid independence study was conducted using four different grid sizes on a plain tube with a 2d-model. The condensing heat transfer coefficients as a function of temperature difference are shown in Fig. 2. These curves in Fig. 2 show that the results agree well with each other. Hence, the grid system with 19,404 elements was adopted and 3D-simulations were performed with the grid system. The gird size is the same as the 2d-model.

4.2. Time-step independence

To analyze the influence of time step on the results, numerical simulations using four different time steps from 10^{-3} s to 5×10^{-5} s were performed for the plain tube with a 2d-model. Fig. 3 indicates that

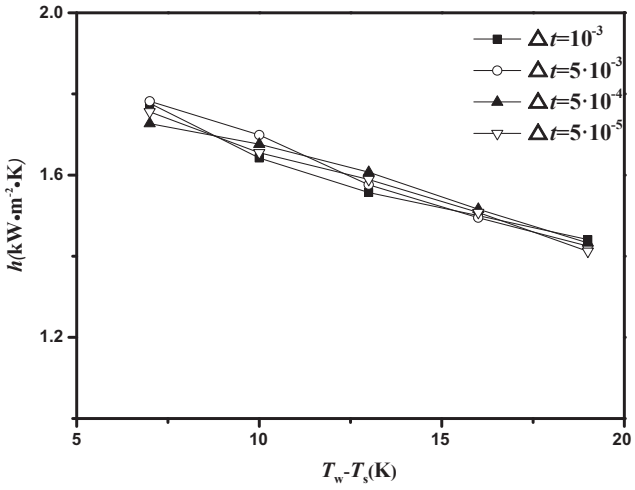

Fig. 3. Variation of the condensing heat transfer coefficient with time step.

the results are absolutely independent of the time step. The time step with 5×10^{-4} s was adopted for the recommended Courant number (Co $<$ 0.25) and 3D-simulations were performed using the same time step.

4.3. Experimental validation

4.3.1. Experimental apparatus and procedures

The experimental system includes three circulating loops: refrigerants, heating and cooling water, which is shown in Fig. 4. The refrigerant circulating system consists of evaporator, condenser, and ducts connecting the two vessels. To ensure the experimental apparatus is well insulated, the rubber material with thickness of 40 mm is used and one layer of aluminum foil is used to enwrap the rubber.

Four tubes can be fixed in the condenser at each experiment. The saturation temperature in the condenser could be adjusted in the range of 1–40 °C. When testing the condensing heat transfer coefficient of condensing tube, the cooling water is flowing through the tubes fixed in the condenser and the heating water is flowing through the tubes fixed in the evaporator to generate the vapor. The vapor is rising upwards from the evaporator. After condensed, liquid refrigerant returns to the evaporator. The heating water and cooling water circulate by two pumps.

The pressure of the condenser vessel is measured by a pressure gauge, whose rang is 0–2.5 MPa with precision of ± 0.00625 MPa. A weight-time flow meter is used to measure the flow rate of cooling water. Five platinum temperature transducers (with a precision of $\pm 0.15 + 0.002|t|$K at the test range) are fixed in the condenser vessel to measure the temperature. Thermocouples are used to test the temperatures of inlet and outlet of cooling water. The thermocouples were calibrated against a temperature calibrator with a precision of ± 0.2 K before experiment. A Keithley digital voltmeter with a resolution of 0.1 μV is used to measure the electrical potential of the sensors.

4.3.2. Experimental procedures

Firstly, high pressure nitrogen, nearly 1.2 MPa, was charged into the whole system after the tubes were fixed in the condenser. To ensure the system being well sealed, tightness check was performed. After all the leaks were eliminated, the system was evacuated to a pressure lower than 800 Pa, and refrigerant was finally charged into the system. The experiment was then conducted. The specifications of test tubes are given in Table 2.

Table 2
Specifications of test tubes in experiment.

Tubes		Outside diameter	Inside diameter	Fin height	Fins pitch
Plain	mm	19.09	16.41	–	–
32-fpi tube	mm	19.06	16.28	1.40	0.79

4.3.3. Data reduction and analysis of uncertainties

The heat balance is firstly examined by comparing the power input and output.

The heat rejection by cooling water is:

$$\phi_{\mathrm{b}} = \mathrm{m}_b c_p (T_{b,1} - T_{b,2}) \tag{13}$$

The heating power input by heating water is:

$$\phi_{\mathrm{c}} = \mathrm{m}_{\mathrm{c}} c_p (T_{c,2} - T_{c,1}) \tag{14}$$

where $T_{\mathrm{b},1}$ and $T_{\mathrm{b},2}$ are the inlet and outlet temperature of heating water (K), $T_{\mathrm{c},1}$ and $T_{\mathrm{c},2}$ are the inlet and outlet temperature of cooling water (K). m_{b} and m_{c} are the mass flow rate of the heating and cooling water (kg/s). c_{p} is the specific heat capacity of water corresponding to the mean temperature of inlet and outlet water (J/kg·K).

The maximum differences between the heat transfer rates of heating and cooling water are within 3%. The average of the two heat transfer rates is used to calculate the overall heat transfer coefficient:

$$k = \frac{\phi}{A_{\mathrm{o}} \cdot \Delta T_m} \tag{15}$$

where A_o is the heat transfer surface area based on the outside diameter of embryo tube, and $\triangle T_m$ is the log-mean temperature difference:

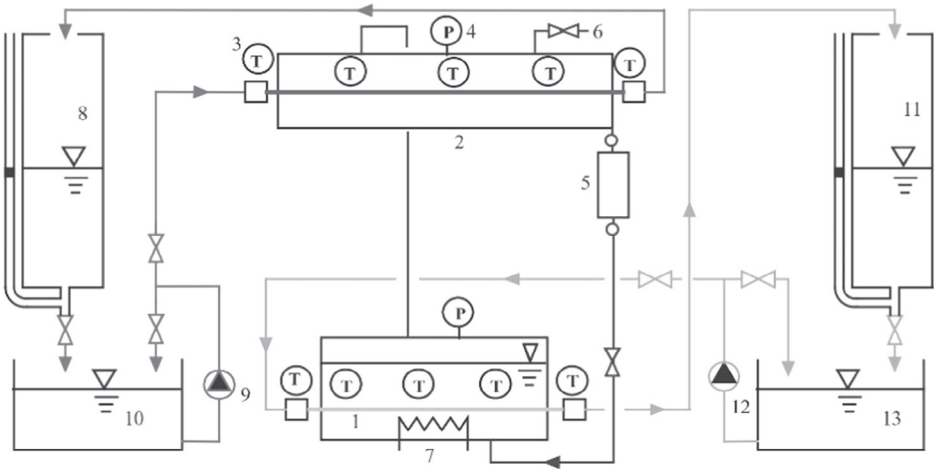

(1) Evaporator;(2)condenser;(3)thermocouple;(4)pressure gauge;(5)condensate measuring container;(6)exhausting valve;(7)subsidiary electric heater;(8)weight-time flow meter of cooling water;(9)cooling water pump;(10)cold water storage tank; (11) weight-time flow meter of heating water; (12)heating water pump; (13)hot water storage tank.

Fig. 4. Schematic diagram of the experimental apparatus.

$$\Delta T_m = \frac{T_{c,2} - T_{c,1}}{\ln \frac{T_s - T_{c,1}}{T_s - T_{c,2}}} \tag{16}$$

where T_s is the saturate temperature. The condensing heat transfer coefficient h_o is obtained with the thermal resistance separation method:

$$\frac{1}{h_o} = \frac{1}{k} - \frac{A_o}{A_i}\frac{1}{h_i} - R_w \tag{17}$$

where R_w is the thermal resistance of the tube wall and A_i is the area of internal tube. h_i is the water side heat transfer coefficient, calculated by Gnielinski correlation.

Experimental uncertainty analysis is made according to [26,27]. For plain and integral-fin tubes, the estimated uncertainties of k are less than 6.8% and 5.3%. h_o is not directly measured and the uncertainties of h_o is estimated with the following method. The uncertainties in calculation h_i are considered to be 10%. The worst situation happens when the overall thermal resistance and that of water side thermal resistance are in the opposite direction. Under such situation, a maximum error of h_o occurs. Therefore, the estimated uncertainties of h_o for plain and integral-fin tubes are 9.9–18.7% and 13.3–33.5%.

4.3.4. Model validation with experimental data

In order to verify the numerical method, the simulations were performed with refrigerants R134a and R11. Although the R11 have been phased out, different property and the behavior of condensate can also supplement the analysis. The properties of these two refrigerants are listed in Table 3. Firstly, comparison between numerical and experimental results are made in terms of R134a. The condensing heat transfer coefficients for plain tube obtained by numerical simulation are compared with the experimental data and Nusselt analytical solution [1]. The expression of Nusselt analytical solution is:

$$h = 0.729\left(\frac{rg\lambda_l^3\rho_l^2}{\mu_l d_o(t_s - t_w)}\right)^{1/4} = 0.656\left(\frac{rg\lambda_l^3\rho_l^2}{\mu_l d_o q}\right)^{1/3} \tag{18}$$

For the plain tube, the condensing heat flux varies from 7 kW·m^{-2} to 30 kW·m^{-2} at saturation temperature of 313 K. As seen in Fig. 5, the relatively deviation of experimental result and numerical result from Nusselt analytical solution is within ± 10%. The deviation between experimental result and Nusselt analytical solution could be caused by the fluctuations of liquid film. As the increase of heat flux, the flow rate of the condensate will also increase. Fluctuation might increase the heat transfer. Nusselt analytical solution is obtained based on eight typical assumptions. It is assumed that the saturate vapor was static and the condensate film flows without any fluctuation. The deviation is chiefly caused by these two factors. As the uncertainties in experiment are always present, this deviation is also inevitable.

The agreement with the analytical solution validates the experimental apparatus and the numerical method. The deviation between the numerical result and Nusselt analytical solution may be caused by the assumptions, such as the negligence of condensation inundation.

For the 32-fpi integral-fin tube, a comparison is made between numerical simulation results and experimental data. Fig. 6 shows the variation of the condensing heat transfer coefficient with heat flux from 13 kW·m^{-2} to 78 kW·m^{-2}. It shows that the numerical simulation results are a little bit lower than experimental results with deviations between 1% and 9%. It can be observed in Fig. 6 that the numerical

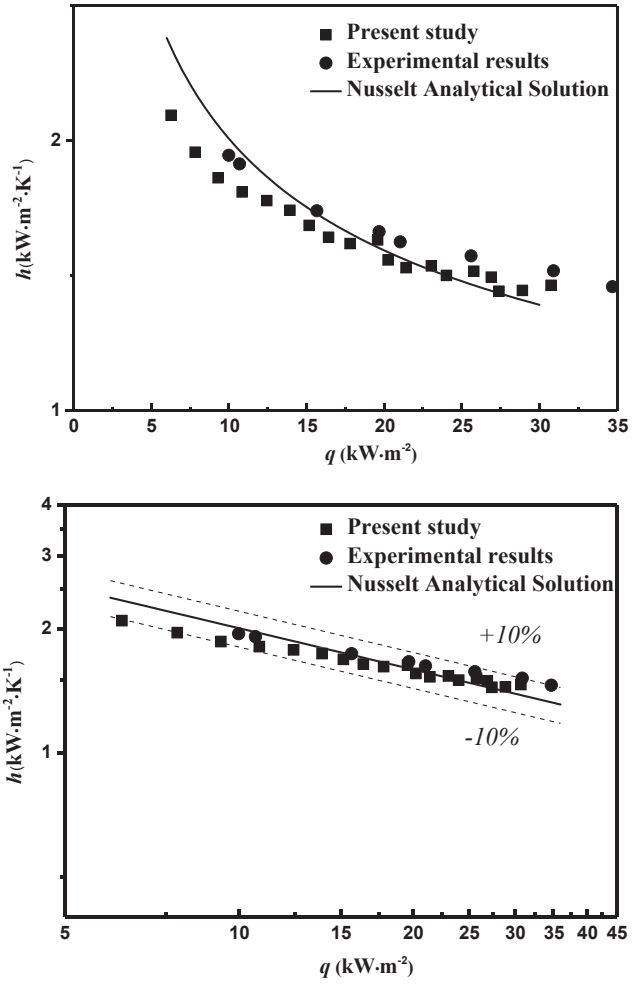

Fig. 5. Comparison of condensing heat transfer coefficient outside the plain tube between numerical results, Nusselt analytical solution and experimental results.

results are lower than the experimental results at lower heat flux (13–40 kW·m^{-2}). At higher heat flux, the numerical results are higher than the experimental results. This result might be caused by the negligence of condensation inundation. The condensation inundation is more pronounced at higher heat flux. The effect of condensation inundation would diminish the heat transfer.

Additionally, numerical simulation results of 32 and 41-fpi tubes are also compared with Cheng and Wang's experimental results [2]. The specifications of the test tubes in Cheng and Wang's work are given in Table 4. In order to investigate the effect of fin pitch on condensing heat transfer coefficient, the diameter and fin height of integral-fin tubes are the same in numerical simulation.

Cheng and Wang used the Wilson plot method with the linear surface tension model of Webb et al. [28] to calculate values of C_n. According to Webb et al. [28], effect of surface tension accounts for one quarter of the heat transfer coefficient. Combining the Wilson plot method and the linear surface tension model of Webb et al. [28] can improve the accuracy of condensing heat transfer coefficient. The C_n is

Table 3
Properties of refrigerant.

	h kJ kg^{-1}	ρ_l kg m^{-3}	ρ_g kg m^{-3}	k_l Wm^{-1} K^{-1}	k_g Wm^{-1} K^{-1}	Cp_l kJ kg^{-1}K^{-1}	Cp_g kJ kg^{-1}K^{-1}	μ_l PaS	μ_g PaS	σ Nm^{-1}
R134A	163.17	1147.4	49.872	0.075	0.0154	1.49	1.14	0.000162	0.0000124	0.00615
R11	177.12	1452.2	8.369	0.0840	0.00889	0.89	0.62	0.00036	0.0000105	0.016

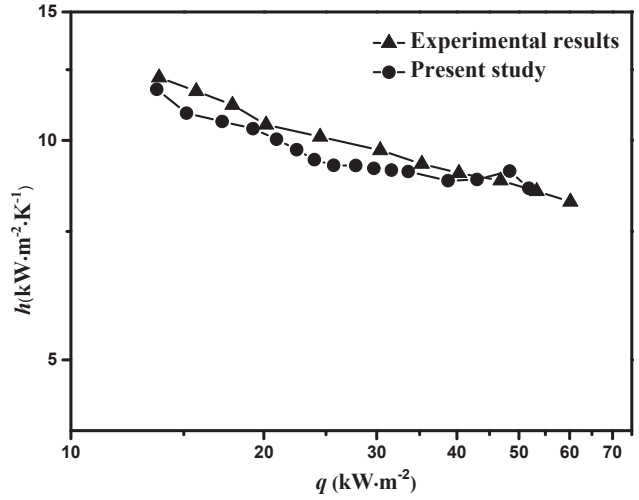

Fig. 6. Comparison of condensing heat transfer coefficient outside the 32-fpi integral-fin tube between numerical results tube and experimental results.

Table 4
Specifications of the tubes in Cheng and Wang's experimental work.

Tubes		Outside diameter	Inside diameter	Fin height	Fin pitch
32-fpi tube	mm	18.26	13.90	1.01	0.79
41-fpi tube	mm	18.80	13.74	1.42	0.61

Table 5
C_n value compared with Cheng and Wang's experimental work.

Tube	C_n in present numerical work	C_n in Cheng and Wang's paper
32-fpi tube	5.88	5.47
41-fpi tube	9.06	8.21

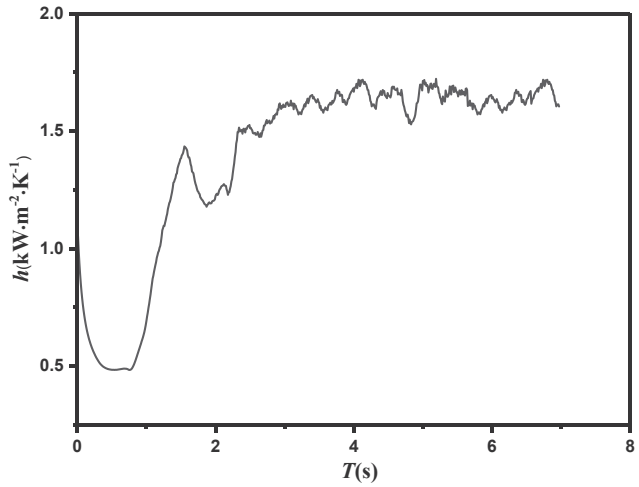

Fig. 7. Variation of the condensing heat transfer coefficient outside plain tube for different time with T_w = 303 K.

the enhanced ratio for the enhanced tubes. It is shown as follows:

$$h = 0.729C_n\left(\frac{rg\lambda_l^3\rho_l^2}{\mu_l d_o(t_s - t_w)}\right)^{1/4} \quad (19)$$

To get enhanced ratio for the integral-fin tubes in present numerical work, we calculate C_n at different heat flux and then take an average. The C_n at different heat flux varies from 5.6 to 6.3 for 32-fpi tube and 8.7 to 9.4 for 41-fpi tube. Table 5 shows the enhanced ratio (C_n) in Cheng and Wang's paper and present numerical study. It is found that the enhanced ratio (C_n) of the 32-fpi and 41-fpi integral-fin tubes is only a little bit higher than that in Cheng and Wang's experimental work.

In this section, the numerical results for the plain tube and integral-fin tubes are compared with Nusselt analytical solution and the experimental data to validate the numerical method. The small deviation indicates that the numerical method can be used to predict the condensing heat transfer coefficient outside the integral-finned tubes.

4.4. Instantaneous film flow characteristics of condensation on plain tube

The condensation and flow of R134a outside the tube is a transient process. The heat flux and condensing heat transfer coefficient are dependent on the time. In this section, the instantaneous film flow characteristics and condensing heat transfer coefficient will be further investigated. Fig. 7 illustrates the variation of the condensing heat transfer coefficient during the condensing process. In Fig. 8, the contours of liquid volume fraction outside plain tube at different time are depicted. Fig. 7 shows that with the passage of time, the condensing heat transfer coefficient firstly decreases, then rises and finally reaches to a relatively steady value. It can be attributed to the process of condensation. As the thickness of liquid film increases, the heat transfer coefficient also decreases. The thickness of liquid film reaches to the maximum value at 0.73 s and the condensing heat transfer coefficient reaches to the minimum value at the same time. Then, with the liquid dripping, the condensing heat transfer coefficient begins to increase and finally it reaches to a relatively steady value. Therefore, the data from 4 s to 6 s was obtained to take an average as condensing heat transfer coefficient. Overall, the variation of the condensing heat transfer coefficient is consistent with the variation of liquid film, which indicates that the condensing heat transfer coefficient is very sensitive to the liquid film. Also, the contours demonstrate that the thickness of liquid film is unstable and this phenomenon during experiment could lead to larger deviations.

4.5. Film flow characteristics of condensate on integral-fin tubes

Fig. 9 shows the contours of liquid volume fraction in the channel between fins for three integral-fin tubes at T_w = 303 K. The contours in Fig. 9 are instantaneous, but the characteristics of liquid film distribution are constant. It is obtained at the stage when the liquid drips continuously. A relatively static distribution of the film in simulation is obtained and the condensing heat transfer coefficient in this stage is also relatively steady. As shown in the figures, due to the effect of surface tension, the liquid film on the surface of the fin is pulled toward the root under the pressure gradient. The liquid film at the upper surface becomes very thin and has a higher heat transfer coefficients. According to Al-Badri et al.'s analytical model [16], the corner of root fin that close to the lateral fin is covered by thick liquid film, so this part is inactive in their model. This phenomenon caused by surface tension can be observed in Fig. 9. The condensing heat transfer coefficient for the lateral fin surface and root fin surface will be discussed in next section. Normally, it is quite difficult to obtain the thickness of the film around the enhanced surface with an experimental approach.

Fig. 9 also shows that as the increase of the fin density, the thickness of the liquid film at the fin root increases. The gravity force makes the liquid flow down and it accumulates at the bottom of the tube, which weakens the heat transfer at the bottom. While, as the overall heat transfer area increases, the heat transfer coefficient is higher for the integral-finned tube with higher fin density.

4.6. Condensing heat transfer coefficient in different lateral fin surface

The general decreasing trends of the condensing heat transfer coefficient with increasing heat flux are illustrated in Fig. 10. It is largely caused by the increasing thickness of the liquid film with the

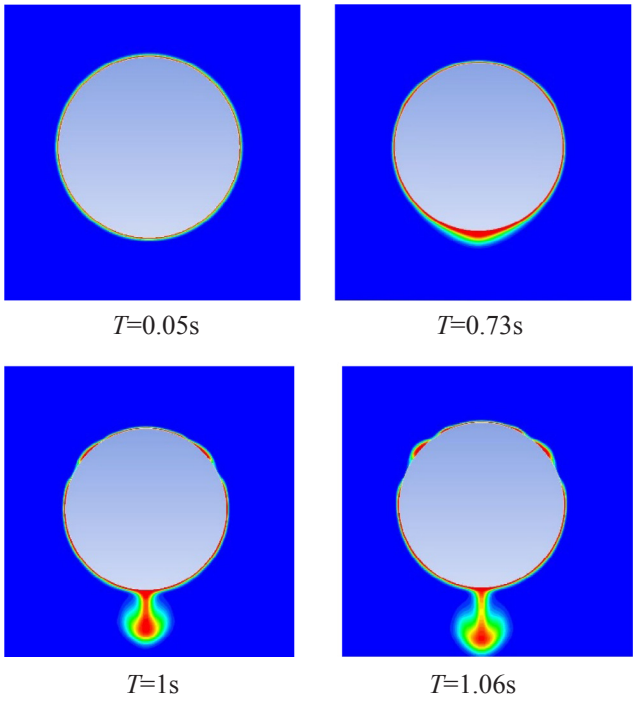

Fig. 8. Contours of liquid volume fraction outside plain tube at different time with T_w = 303 K.

increasing heat flux. The results also show that the condensing heat transfer coefficient is very sensitive to the fin density (fin pitch), which is consistent with the experimental data of Cheng and Wang [2]. The increased heat transfer coefficient for the tubes with higher fin density is chiefly caused by the combined effect of increased heat transfer area and surface tension. In the simulation, the uniform tube wall temperature was given and then the heat flux was determined. For 26, 32, 41-fpi tube, the tube temperature is all set from 293 K to 309 K. As the 26 fpi tube has lower heat transfer coefficient, it has the minimum range of heat flux.

Fig. 11 shows the variations of the condensing heat transfer coefficient with respect to temperature difference, fin density and different part of fin. The plot indicates that as the temperature difference increases, the condensing heat transfer coefficient of the tube, the lateral fin surface and the fin root surface all decrease.

As discussed previously, due to surface tension, the liquid film which acts as an obstacle to heat transfer accumulated at the fin root surface. As a result, the condensing heat transfer coefficient of the root fin surface is much smaller than that of the lateral fin surface. Liquid condensate adhension outside different part of fins plays an important role in the condensing heat transfer. The condensing heat transfer coefficient in the fin root was only one half of the lateral fin surface. Condensate film being drained by the pull-off of surface tension is rather important in improving the heat transfer. The mechanism of heat transfer enhancement for integral-fin tube can be divided into two part: the increase of heat transfer area and thinning of liquid film at lateral fin surface. Using the method of the present study, it can be used to analyze at what fin sizes the surface tension first becomes dominant. In order to take full advantage of the Gregorig effect, it can also be used to obtain the optimum spacing of the fins and design fin structure to provide the adequate condensate drainage.

4.7. Condensation of other refrigerant

In order to validate the present method, the experimental result of R11 was also compared. Although the R11 have been phased out, the behavior of condensate and heat transfer can also be used for the analysis. For refrigerant R11, condensation heat transfer coefficient outside 35 fpi and 26 fpi tubes from literature [14] is compared with

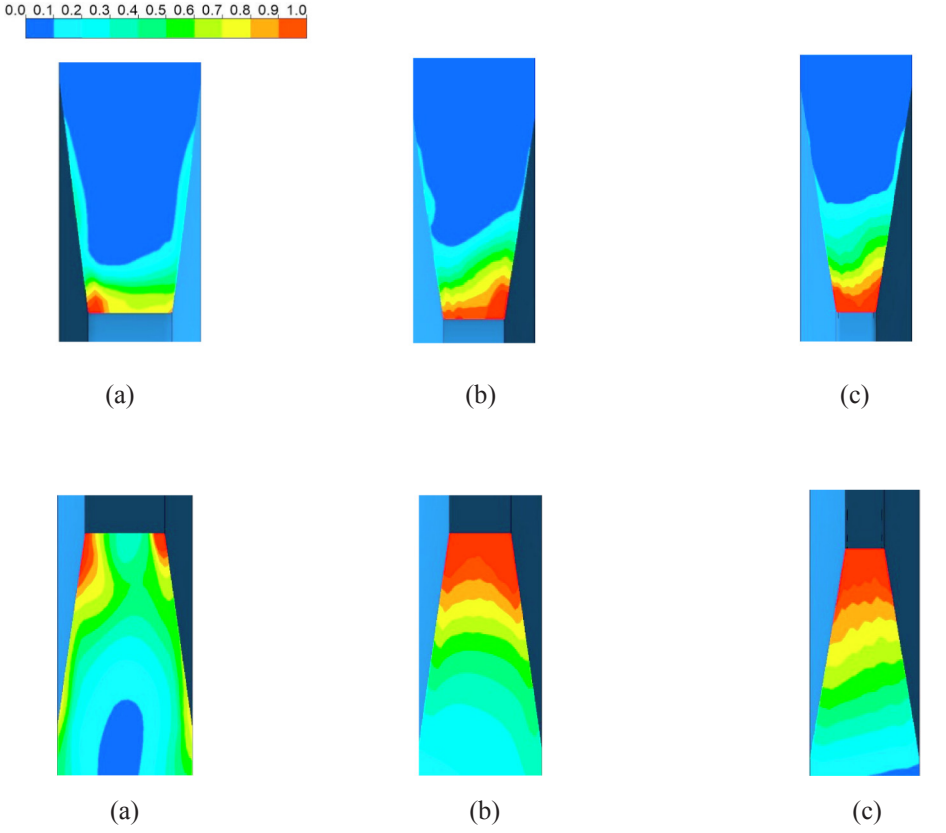

Fig. 9. Contours of liquid volume fraction outside integral-fin tube. Contours of liquid volume fraction in the channel between fins at the top of the tube with T_w = 303 K, (a) 26 fpi-tube; (b) 32 fpi-tube; (c) 41 fpi-tube. Contours of liquid volume fraction in the channel between fins at the bottom of the tube with T_w = 303 K, (a) 26 fpi-tube; (b) 32 fpi-tube; (c) 41 fpi-tube.

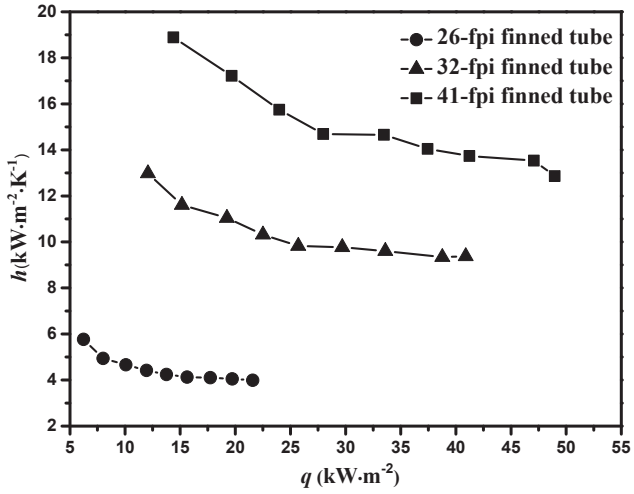

Fig. 10. Variation of condensing heat transfer coefficient with respect to heat flux and fin pitch.

present numerical results in Figs. 12 and 13. It can be found that a favorable agreement is obtained between numerical and experimental results. The condensation heat transfer coefficients of numerical simulation are both lower than that in experiment. The condensation heat transfer coefficient of 32 fpi tube is lower than 35 fpi tube by almost 25%. It was mostly caused by the difference of fin pitch. The model itself may also under-predict the condensation heat transfer coefficient.

It can be observed that the R11 has higher condensation heat transfer performance than R134a. As shown in Table 3, the latent heat of R11 is higher than R134a, which plays an important role for the heat transfer rate. Additionally, the surface tension of R11 is higher than R134a. This could result in different liquid film distribution. The contact angle θ can be obtained by Young's equation [29].

$$\cos\theta = (\gamma_{SV} - \gamma_{SL})/\gamma_{LV} \tag{20}$$

where the subscripts SV and SL refer to the solid interfacing of vapor and liquid; γ_{LV} denotes the interfacial tension between the liquid and vapor. According to the equation, for hydrophilic liquid ($\cos\theta > 0$), the larger the surface tension, the larger the contact angle is. R134a is more hydrophilic than R11. According to Hou et al. [30], the hydrophobicity can aid to the running off of liquid droplet. Compared with R134a, it is easier for R11 to run off from the tube wall.

Fig. 13 shows the contours of liquid film distribution outside the

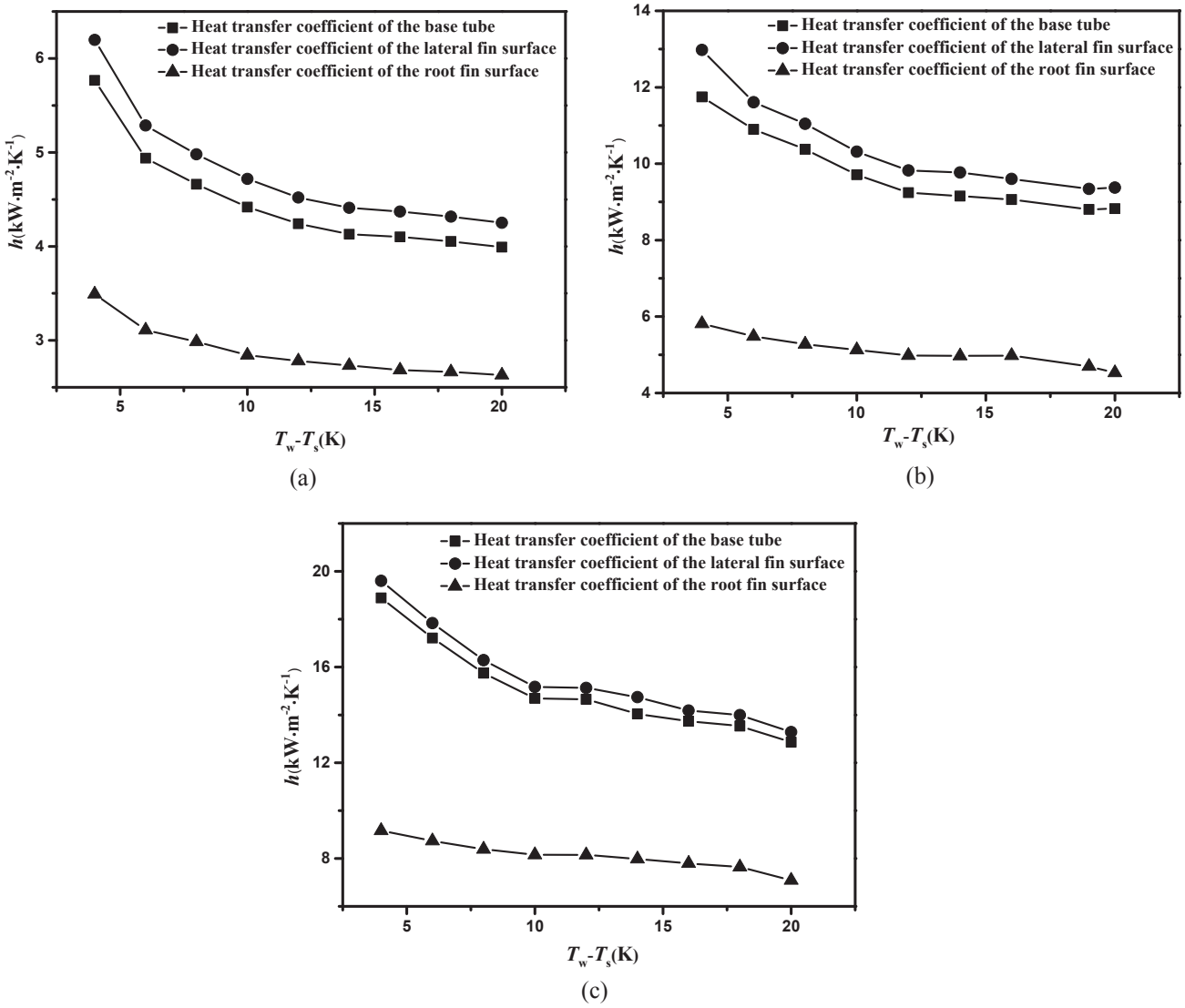

Fig. 11. Variations of condensing heat transfer coefficient for different part and temperature difference: (a) 26-fpi; (b) 32-fpi; (c) 41-fpi.

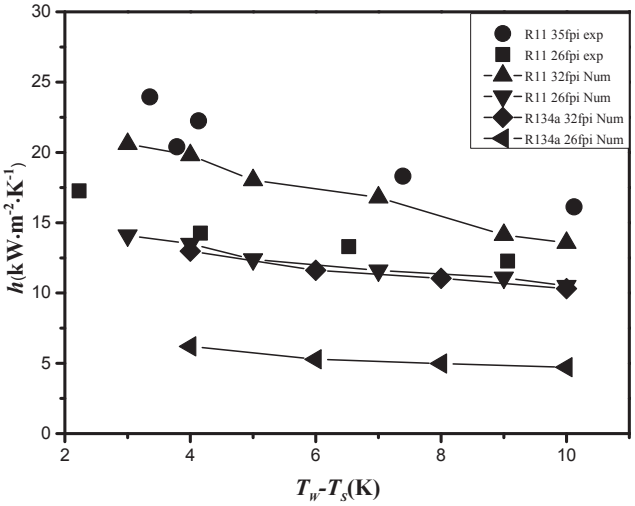

Fig. 12. Comparison of condensing heat transfer coefficient between R134a and R11.

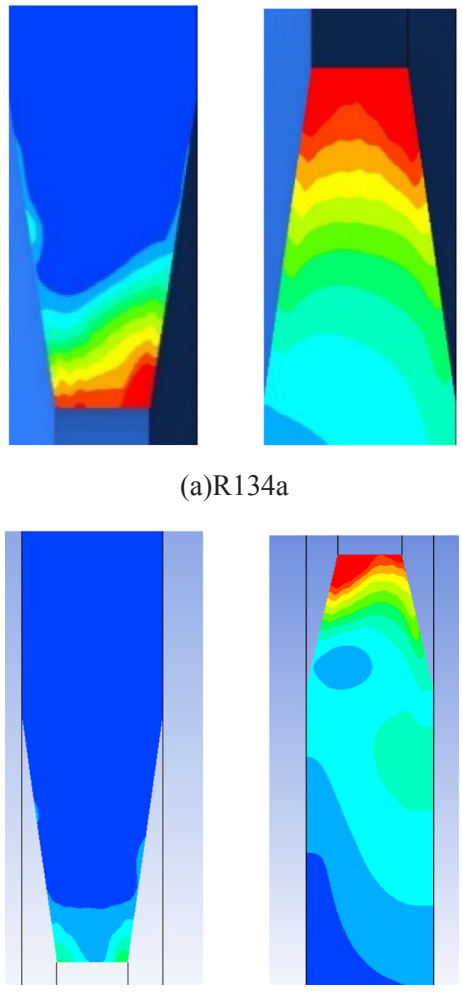

Fig. 13. Contours of liquid volume fraction in the channel at same heat flux, (a) R134a, (b) R11.

fins. It can be observed that the liquid film of R11 at the upper tube is thinner than that of R134a. While at the bottom of the tube, it is thicker than that of R134a. This phenomenon indicates that R11 refrigerant drains more easily compared with R134a. The relatively large surface tension of R11 provides better performance in reducing the thickness of condensate. While R134a condensate may be kept over the fin gaps, which would diminish the condensing heat transfer.

5. Conclusion

In this paper, numerical simulation was performed using the VOF and Lee model. The condensing heat transfer coefficient for the plain and integral-fin tubes was calculated in comparison with the experimental result. The distribution of liquid film on the fin was presented to investigate the mechansim of heat transfer enhancement. Although this article only provides the simulations for the typical integral-low fin tubes, it can also be used for the simulation of other tubes with integral-fins. According to the results, following conclusions can be drawn:

(1) The numerical results of the plain tube and 32-fpi tube agree well with the Nusselt analytical solution and the experimental data. The variation of the condensing heat transfer coefficient is also consistent with experimental result. This method can be used to analyze the condensing heat transfer of integral-fin tubes.
(2) For all enhanced tubes, an increase in the condensing heat transfer coefficient was observed with increasing fin density (decreasing fin pitch). For enhanced tubes, an increase in the film thickness at root fin surface was observed with increasing fin density. It can be found that the film thickness at the bottom of tube is much larger than that in other place.
(3) The local condensing heat transfer coefficient is very sensitive to the film distribution. The unstable thickness of liquid film results in variation of condensing heat transfer coefficient during condensation. The condensing heat transfer coefficient for lateral fin surface is much bigger than that for root fin surface because of smaller liquid film thickness at lateral fin surface. The most important mechansim of heat transfer enhancement for integral-fin tubes is thinning of liquid film at lateral fin surface.
(4) For R11 refrigerant, large surface tension could result in quickly draining of condensate and reduce the thickness of liquid film. The combined effect of latent heat and surface tension contribute to the higher condensation heat transfer coefficient of R11.

Acknowledgment

This work was supported by the National Natural Science Foundation of China (51776160) and National Key Research and Development Program of China (2016YFB0601204).

References

[1] W. Nusselt, The surface condensation of water vapour, Zeitschrift Des Vereines Deutscher Ingenieure 60 (1916) 541–546.
[2] W.Y. Cheng, C.C. Wang, Condensation of R-134a on enhanced tubes, ASHRAE Trans. 100 (part 2) (1994) 809–817.
[3] D. Zhang, W. Ji, J. Du, Z. Zhang, X. Fan, Y.L. He, W.Q. Tao, Parameter comparison of condensation heat transfer of r134a outside horizontal low-finned tubes, IHTC-15(2014), Kyoto, Japan.
[4] W.T. Ji, M. Numata, Y.L. He, W.Q. Tao, Nucleate pool boiling and filmwise condensation heat transfer of R134a on the same horizontal tubes, Int. J. Heat Mass Transf. 86 (2015) 744–754.
[5] W.-T. Ji, C.-Y. Zhao, J. Lofton, Z.-Y. Li, D.-C. Zhang, Y.-L. He, W.-Q. Tao, Condensation of r134a and r22 in shell and tube condensers mounted with high-density low-fin tubes, J. Heat Transf. 140 (2018) 091503–091511.
[6] D. Gstoehl, J.R. Thome, Film condensation of R-134a on tube arrays with plain and enhanced surfaces: Part I – experimental heat transfer coefficients, J. Heat Transf. 128 (2006) 21–32.
[7] A.R. Al-Badri, A. Bär, A. Gotterbarm, M.H. Rausch, A.P. Fröba, The influence of fin structure and fin density on the condensation heat transfer of R134a on single finned tubes and in tube bundles, Int. J. Heat Mass Transf. 100 (2016) 582–589.
[8] K.J. Park, G.K. Dong, D. Jung, Condensation heat transfer coefficients of R1234yf on plain, low fin, and Turbo-C tubes, Int. J. Refrig. 34 (2011) 317–321.
[9] T. Gebauer, A.R. Al-Badri, A. Gotterbarm, J.E. Hajal, A. Leipertz, A.P. Fröba, Condensation heat transfer on single horizontal smooth finned tubes and tube

bundles for R134a and propane, Int. J. Heat Mass Transf. 56 (2013) 516–524.
[10] C.-Y. Zhao, W.-T. Ji, P.-H. Jin, Y.-J. Zhong, W.-Q. Tao, The influence of surface structure and thermal conductivity of the tube on the condensation heat transfer of R134a and R404A over single horizontal enhanced tubes, Appl. Therm. Eng. 125 (2017) 1114–1122.
[11] D.Q. Kern, Mathematical development of tube loading in horizontal condensers, Aiche J. 4 (1958) 157–160.
[12] K.O. Beatty, D.L. Katz, Condensation of vapors on outside of finned tubes, Chem. Eng. Prog. 44 (1948) 908–914.
[13] H. Honda, B. Uchima, S. Nozu, H. Nakata, T. Fujii, Condensation of downward flowing R-113 vapor on bundles of horizontal smooth tubes, Heat Transf. – Jpn. Res. 18 (1989) 31–52.
[14] R.L. Webb, T.M. Rudy, M.A. Kedzierski, Prediction of the condensation coefficient on horizontal integral-fin tubes, J. Heat Transf. 107 (1985) 369–376.
[15] Keiji Murata, Kenichi Hashizume, Prediction of condensation heat transfer coefficient in horizontal integral-fin tube bundles, Exp. Heat Transf. 5 (1992) 115–130.
[16] A.R. Al-Badri, T. Gebauer, A. Leipertz, A.P. Fröba, Element by element prediction model of condensation heat transfer on a horizontal integral finned tube, Int. J. Heat Mass Transf. 62 (2013) 463–472.
[17] C.W. Hirt, B.D. Nichols, Volume of fluid (VOF) method for the dynamics of free boundaries, J. Comput. Phys. 39 (1981) 201–225.
[18] B.D. Nichols, C.W. Hirt, R.S. Hotchkiss, SOLA-VOF: A solution algorithm for transient fluid flow with multiple free boundaries, Nasa Sti/recon Technical Report N 81 (1980).
[19] J.U. Brackbill, D.B. Kothe, C. Zemach, A Continuum Method for Modeling Surface Tension, Academic Press Professional Inc, 1992.
[20] H.L. Wen, A pressure iteration scheme for two-phase flow modeling, Multiphase Transport: Fundamentals, Reactor Safety, Applications, 1980, pp. 407–431.
[21] G. Qiu, Z. Xu, W. Cai, Y. Jiang, Numerical study on the condensation flow and heat transfer characteristics of hydrocarbon mixtures inside the tubes of liquefied natural gas coil-wound heat exchangers, Appl. Therm. Eng. 140 (2018) 775–786.
[22] J. Yu, Y. Jiang, W. Cai, F. Li, Numerical investigation on flow condensation of zeotropic hydrocarbon mixtures in a helically coiled tube, Appl. Therm. Eng. 134 (2018) 322–332.
[23] I. Tanasawa, Advances in condensation heat transfer, in: J.P. Hartnett, T.F. Irvine, Y.I. Cho (Eds.), Advances in Heat Transfer, vol. 21, Elsevier, 1991, pp. 55–139.
[24] E.D. Riva, D.D. Col, Numerical simulation of laminar liquid film condensation in a horizontal circular minichannel, J. Heat Transf. 134 (2012) 051019.
[25] B. Van Leer, Towards the ultimate conservative difference scheme: A second-order sequel to Godunov's method, J. Comput. Phys. 32 (1979) 101–136.
[26] R.J. Moffat, Describing the uncertainties in experimental results, Exp. Therm. Fluid Sci. 1 (1988) 3–17.
[27] B. Cheng, W. Tao, Experimental-study of r-152a film condensation on single horizontal smooth tube and enhanced tubes, J. Heat Transfer-Trans. ASME.
[28] R.L. Webb, S.T. Keswani, T.M. Rudy, Investigation of surface tension and gravity effects in film condensation, Proc. 7th Int. Heat Transfer Conference, Washington, DC,.U, 5 1982, pp. 175–180.
[29] D. Sullivan, Surface tension and contact angle of a liquid–solid interface, J. Chem. Phys. 74 (1981) 2604–2615.
[30] H. Youmin, Y. Miao, C. Xuemei, W. Zuankai, Y. Shuhuai, Recurrent filmwise and dropwise condensation on a beetle mimetic surface, ACS Nano. 9 (2015) 71.